

Annemarie van Schaik
First supervisor: Geeske van Woerden, Erasmus MC
Second supervisor: Harold MacGillavry, Utrecht University
Daily supervisor: Pomme Rigter, Erasmus MC
Minor internship/general research profile

Resolving the effect of Shank3 S1510 phosphorylation on Shank3 functioning

Layman's summary

In de hersenen liggen miljoenen hersencellen, ook wel neuronen genoemd. Deze neuronen ontvangen signalen vanuit het lichaam of vanuit andere neuronen, en geven ze op hun beurt weer door aan nieuwe neuronen. Neuronen geven die signalen door via synapsen. Een synaps bestaat uit een presynaps op het gevende neuron, en een postsynaps op het ontvangende neuron. De presynaps laat moleculen, genaamd neurotransmitters, los die vervolgens aan receptoren in de postsynaps binden. Deze receptoren liggen in een structuur helemaal vol met eiwitten, genaamd de postsynaptische dichtheid (PSD). De vele eiwitten hier hebben allerlei verschillende functies, waaronder het vastzetten van de receptoren, het verwerken van signalen, of zorgen voor vorm en stevigheid. De connectie tussen de pre- en de postsynaps kan sterker en zwakker worden, dit heet plasticiteit. Het sterker worden van de connectie kan onder andere veroorzaakt worden door aanhoudende activatie vanuit de presynaps, en kan lange termijn potentiatie (LTP) veroorzaken. Tijdens LTP komen er onder andere meer receptoren naar de PSD, en kan de PSD ook groter worden. Een belangrijk eiwit in de PSD is Shank3. Door vele interacties aan te gaan met andere eiwitten zorgt Shank3 ervoor dat eiwitten op zijn plek blijven zitten in de PSD. Shank3 is relatief vaak betrokken in meerdere neurologische aandoeningen zoals autisme, daarom is onderzoek naar Shank3 belangrijk. Shank3 kan geactiveerd worden door fosforylatie. Als een eiwit gefosforyleerd wordt, wordt er een fosfaatgroep aangezet wat resulteert in een verandering in activiteit. Als een synaps LTP ondergaat worden er veel eiwitten gefosforyleerd, wat dus kan zorgen voor versterking van de connectie tussen pre- en postsynaps. Recentelijk is er een nieuwe fosforylatie plek gevonden op Shank3, waarvan gedacht wordt dat het een belangrijke rol kan hebben in de regulatie van Shank3 activatie. Het is echter nog niet bekend wat het precieze effect van deze fosforylatie op Shank3 is. In dit project zijn een aantal experimenten uitgevoerd om hierachter te komen. Daarvoor zijn twee Shank3 varianten ontwikkeld. Eén waarin de fosforylatie nagebootst wordt zodat het lijkt alsof Shank3 constant gefosforyleerd wordt op deze plek, en één waar Shank3 niet gefosforyleerd kan worden op deze plek. De verschillen in resultaten tussen deze twee varianten en de normale Shank3 laten zien wat het effect is van deze fosforylatie. We laten zien dat het aannemelijk is dat, ondanks dat fosforylatie vaak betrokken is bij LTP, dit voor deze fosforylatie op Shank3 niet het geval is. De resultaten laten een klein verschil zien in de rekrutering van Shank3 in en uit de postsynaps na LTP, maar dit verschil is te klein om definitieve conclusies uit te trekken. Daarnaast wordt in dit project ook aangetoond dat deze fosforylatie wellicht een effect heeft op de interactie tussen Shank3 en een aantal andere eiwitten. Echter, ondanks wat kleine verschillen, alle resultaten bij elkaar laten zien dat het aannemelijk is dat deze specifieke fosforylatie van Shank3 niet zo belangrijk is als van tevoren gedacht.

Abstract

Shank3 is an important scaffolding protein in the postsynaptic density (PSD). It functions in forming multiple complexes that anchor receptors, but also in connecting the PSD to the Actin cytoskeleton. Shank3 has many phosphorylation sites. Recently, it has been shown in a double CaMKIIa/b knockout that the phosphorylation levels of Shank3 are strongly decreased, suggesting that CaMKII is an important kinase in Shank3 phosphorylation. In this phospho-proteomics study, Serine 1510 came forward as an important phosphorylation site on Shank3, likely phosphorylated by CaMKII. Here, by using a phospho-dead (S1510A)

and phospho-mimic (S1510D) mutation, we attempted to find the effect of S1510 phosphorylation on Shank3 functioning. As it is likely that CaMKII is involved in this phosphorylation and since it is known that CaMKII is highly involved in long term potentiation (LTP), we tested the effects of S1510 phosphorylation in LTP. We show that S1510 phosphorylation does not affect spine number, spine morphology, or GluA2 membrane levels after inducing LTP. A small trend in Shank3 recruitment after LTP, where S1510A has an increased Shank3 size and intensity in the spine, whereas in S1510D these are both decreased, suggests that S1510 phosphorylation possibly affects Shank3 recruitment after LTP. Lastly, we also show that S1510 phosphorylation likely does not affect Shank3 oligomerization nor the interaction between Shank3 and Homer. The interaction between Shank3 and Cortactin, Rich2, and GKAP, are possibly affected. All together we show that, based on our data, S1510 phosphorylation is presumably not as important as previously thought for the regulation of Shank3.

Introduction

Neurotransmitters released from the presynapse bind to receptors in the postsynapse. These receptors are localized in the postsynaptic density (PSD), a dense protein structure which is localized right underneath the postsynaptic membrane (Boeckers, 2006). Receptors in the PSD are activated upon neurotransmitter binding, which causes an ion influx into the postsynapse, leading to signal processing in the PSD and transmission to the rest of the neuron. Persistent activation of these receptors caused by repeated neurotransmitter release generates a Ca^{2+} influx in the postsynapse, which activates multiple processes in the PSD that can lead to long-term potentiation (LTP). During LTP, the synaptic connection gets stronger (Citri & Malenka, 2008). The Ca^{2+} influx activates Ca^{2+} /Calmodulin-dependent protein kinase II (CaMKII), a kinase that phosphorylates multiple other proteins upon activation and thereby has an important function in initiating LTP (Lisman et al., 2012). LTP has multiple effects, including but not limited to, an increased number of receptors in the PSD, Actin remodeling which generates the growth of spine head size, and stimulation of spine maturation leading to more filopodium spines (Herring & Nicoll, 2016). The PSD has an important function in LTP: besides functioning in neuronal transmission and the induction of LTP, proteins in the PSD also regulate the trafficking and anchoring of receptors or they balance structural changes by coupling the PSD to the Actin cytoskeleton (Murakoshi & Yasuda, 2012).

An important protein in the PSD is Shank3. (Perfitt, Wang, et al., 2020). Shank3 is part of the Shank family of scaffolding proteins, of which Shank3 is the best studied (Sheng & Kim, 2000). It is a large PSD protein, which functions mostly in scaffolding many other proteins such as Cortactin (MacGillavry et al., 2016), GKAP (Naisbitt et al., 1999), and Homer (Tu et al., 1999). Shank3 consists of five domains through which it interacts with its interaction proteins (Monteiro & Feng, 2017), and through which it also oligomerizes (Naisbitt et al., 1999). Besides anchoring proteins, Shank3 is part of numerous bigger complexes in the PSD, for instance with GKAP and PSD-95 that anchors NMDA receptors (Naisbitt et al., 1999). Furthermore, it links the PSD to the Actin cytoskeleton via its interaction with various Actin remodeling proteins like Cortactin and α -Fodrin (Sarowar & Grabrucker, 2016). Shank3 is involved in multiple neurological disorders like Phelan McDermaid syndrome, Intellectual Disability (ID), and Autism Spectrum Disorder (ASD) (Wan et al., 2021). Multiple studies with Shank3 mutations or mice lacking Shank3 show deficits in synaptic transmission and LTP (Bozdagi et al., 2010; Kouser et al., 2013). Therefore, it is of great importance to unravel the function of Shank3 in the brain.

It is known that Shank3 has many phosphorylation sites (Wang et al., 2020) and that it is phosphorylated by CaMKII (Perfitt, Stauffer, et al., 2020). Recently, in double knock-out mice for CaMKII isoforms CaMKII α and CaMKII β (Kool et al., 2019), a study shows that Shank3 phosphorylation levels are strongly decreased (unpublished data). This suggests that CaMKII is an important kinase in regulating the phosphorylation levels of Shank3, thereby regulating Shank3 activation. In this phospho-proteomics study, Serine 1510 (S1510) came forward as an important site in Shank3 that is phosphorylated, very likely by CaMKII. This phosphorylation site has been reported before in a mass-spectrometry study (Wang et al., 2020), however the function of this

S1510 phosphorylation site is not known. In this project, we seek to resolve this using the research question “What is effect of S1510 phosphorylation on Shank3 functioning?”.

We tested the effect of S1510 phosphorylation on spine morphogenesis, Shank3 size and localization, and AMPA receptor exocytosis, all in basal state and after inducing LTP. Next to that, we tested the interaction efficiency between Shank3 and a selection of its interaction proteins. We show that S1510 phosphorylation only has a small effect on Shank3 structure size and localization after inducing LTP, and that the interaction efficiency between Shank3 and GKAP, Rich2, and Cortactin are possibly affected. Despite the fact that this phosphorylation site came forward as possibly important for Shank3 regulation based on the phospho-proteomics study, we do not find an important function for S1510 phosphorylation in the Shank3 functions tested here.

Results

S1510 mutations do not affect the number of spines nor their morphology

To study the effect of Shank3 S1510 phosphorylation, we designed and cloned two mutations at S1510. We mutated S1510 to Aspartic Acid (D), which is a negatively charged amino acid and mimics the negative charge of a phosphate group. This is used as a phospho-mimic mutation. As a negative control, we mutated S1510 to Alanine (A), which is a neutral amino acid that cannot be phosphorylated. Shank3 constructs with these mutations were placed in a vector also containing a tdTomato plasmid under a different promoter. As a control, an empty vector (EV) was used, consisting only the tdTomato plasmid and no Shank3 construct. We transfected primary mouse hippocampal neurons with one of these constructs at DIV 10 or 11. Chemical LTP (cLTP) was induced at DIV15, using glycine as described in methods. We stained for Shank3, and additionally also Synapsin is stained as a synapse marker. Neurons were visualized using Confocal microscopy (Zeiss).

Looking at the dendrites, overexpressing Shank3 did not affect neuronal appearance at first sight (fig. 1A). Also the phospho-dead (S1510A) and phospho-mimic (S1510D) mutations did not cause visible defects (fig. S1C+E). As Shank3 is involved in spine formation and maturation (Sala et al., 2001), we analysed if the S1510 mutations affected the number of spines in the neuron in basal state and after inducing cLTP. Neurons transfected with Shank3 WT had 10.5 ± 0.72 spines per $20 \mu\text{m}$ dendrite (fig 1A+I), which is comparable to the EV (9.4 ± 0.43 ; fig. 1I+S1A). S1510A, the phospho-dead mutation, caused the neurons to have significant less spines compared to WT (8.6 ± 0.21 ; $p < 0.05$; fig. 1I+S1C). The phospho-mimic mutation S1510D did not cause a significant change in number of spines compared to WT (8.8 ± 0.71 ; $p > 0.05$; fig. 1I+S1E) or S1510A phospho-dead ($p > 0.05$; fig. 1I), although we noticed a decreasing trend. Inducing LTP is known to increase the number of spines (Engert & Bonhoeffer, 1999; Maletic-Savatic et al., 1999). However, we observed no increase in spines in WT (9.9 ± 0.53 ; $p > 0.05$; fig. 1B+I) nor in EV (10.1 ± 0.56 ; $p > 0.05$; fig. 1I+S1B) after inducing cLTP. We did observe an increase in number of spines in the S1510A phospho-dead mutation (10.7 ± 0.61 ; $p < 0.05$; fig. 1I+S1D) as well as in the S1510D phospho-mimic mutation (11.2 ± 0.6 ; $p < 0.05$; fig. 1I+S1F).

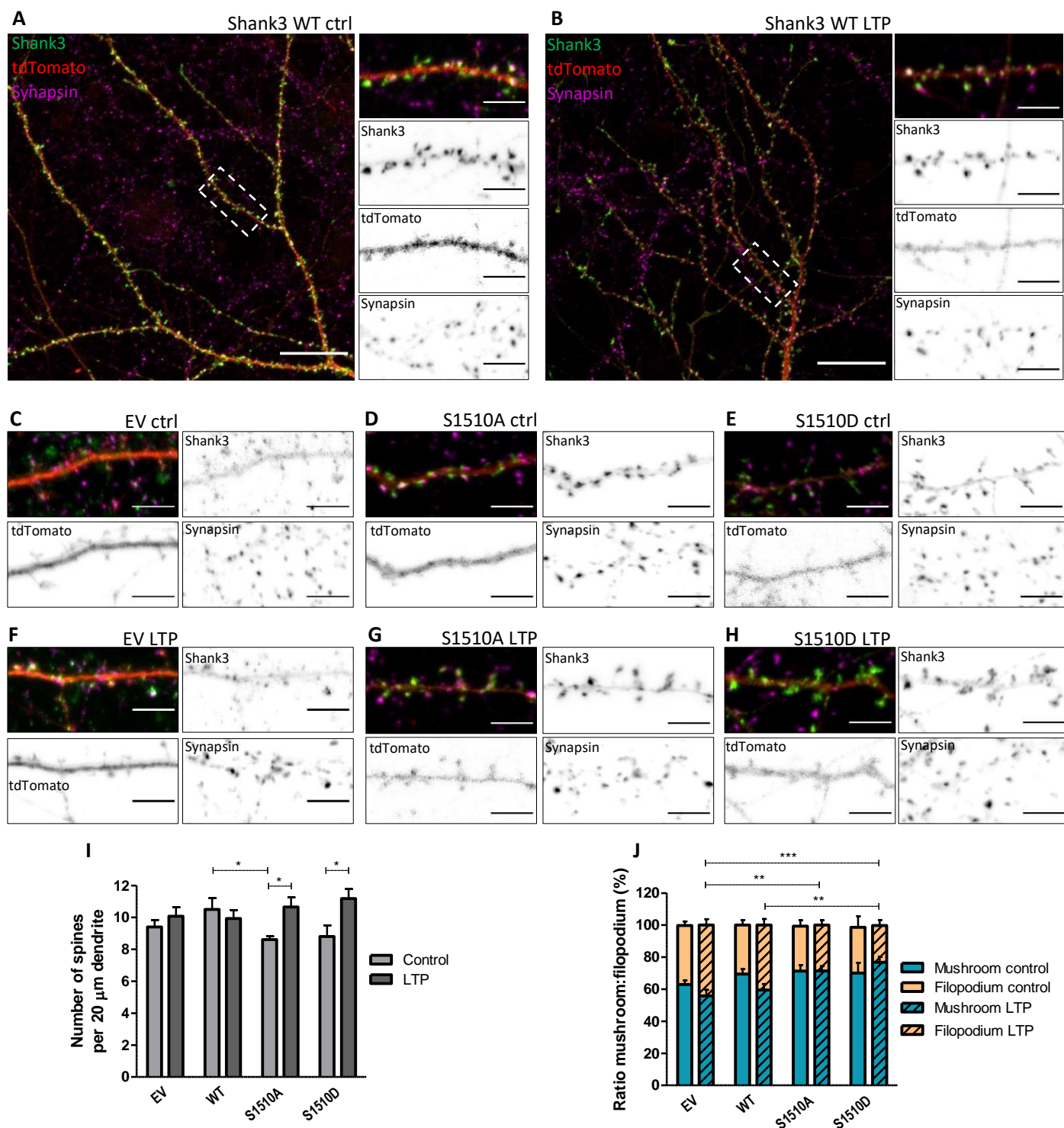


Figure 1. S1510 phosphorylation mutations do not affect spine number and morphology

A: Neuron expressing Shank3-WT construct (green) and tdTomato (red), stained for Synapsin (magenta). Dotted rectangle represents the zoom in of the dendrite on the right. Scale bar 20 μ m for the whole neuron, 5 μ m for the zoomin

B: Neuron expressing Shank3-WT construct (green) and tdTomato (red), stained for Synapsin (magenta), induced for cLTP. Dotted rectangle represents the zoom in of the dendrite on the right. Scale bar: 20 μ m for the whole neuron, 5 μ m for the zoomin

C-F: Dendrite of a neuron expressing EV construct with tdTomato (red), stained for Shank3 (green) and Synapsin (magenta). Scale bar: 5 μ m

D, E, G, H: Dendrite of a neuron expressing a Shank3 construct (green) and tdTomato (red), stained for Synapsin (magenta). Scale bar: 5 μ m.

I: Quantification of number of spines per 20 μ m dendrite for all conditions, shown as mean + SEM.

J: Quantification of spine morphology ratio mushroom:filopodium shown as mean + SEM. I+J number of neurons: EV ctrl n=8; EV LTP n=9; WT ctrl n=9; WT LTP n=7; S1510A ctrl n=10; S1510A LTP n=10; S1510D ctrl n=6; S1510D LTP n=10

Next, we looked at the morphology of spines. It is known that LTP induces spine maturation, thereby changing spine morphology from filopodium to mushroom (Murakoshi & Yasuda, 2012). Shank3 is also known to be involved in inducing spine maturation (Sala et al., 2001), therefore we wanted to know if the spine ratio mushroom:filopodium would be affected by the S1510 phosphorylation mutations in basal state or after inducing cLTP. The ratio mushroom:filopodium for all conditions is shown in fig. 1J, and was similar between EV ($62.9 \pm 2.54\%$: $36.8 \pm 2.62\%$) and WT ($69.4 \pm 3.10\%$: $30.6 \pm 3.10\%$). The S1510A phospho-dead mutation ($71.2 \pm 3.78\%$: $28.1 \pm 3.70\%$) as well as the phospho-mimic mutation ($70.0 \pm 6.42\%$: $28.6 \pm 6.89\%$) did not affect the spine morphology ratio compared to WT (both $p > 0.05$). Surprisingly after inducing cLTP, we did not observe a shift in mushroom:filopodium spine ratio for EV ($55.8 \pm 3.74\%$: $44.2 \pm 3.74\%$) nor for WT ($59.5 \pm 3.77\%$: $40.5 \pm 3.77\%$). On the contrary, we did observe a shift for both S1510 phosphorylation mutations after inducing cLTP: $71.3 \pm 2.99\%$: $28.7 \pm 2.99\%$ for the S1510A phospho-dead mutation and $76.8 \pm 3.38\%$: $23.0 \pm 3.31\%$ for the S1510D phospho-mimic mutation. Both mutations shifted significantly towards mushroom compared to WT after inducing cLTP (both $p < 0.05$).

Together, these results demonstrate that overexpressing Shank3 does not affect the number of spines nor the spine morphology ratio, as there are no changes between EV and WT. The results also show that the number of spines are decreased in basal state in both S1510 phosphorylation mutations, and increased in both mutations after inducing cLTP. Furthermore, the results show that after inducing cLTP, the spine morphology ratio does not change in EV and WT, and shift towards mushroom in both S1510 phosphorylation mutations.

Shank3 size and localization are slightly altered by S1510 phosphorylation mutations after LTP

To find out if S1510 phosphorylation affects Shank3 structure size and localization in the PSD, we analysed the size of Shank3 structures in the spine in basal state and after inducing cLTP (fig. 2A). We found that in basal state S1510A phospho-dead ($0.458 \pm 0.042 \mu\text{m}^2$) and S1510D phospho-mimic mutations ($0.496 \pm 0.029 \mu\text{m}^2$) both show a small increase in size compared to WT ($0.378 \pm 0.037 \mu\text{m}^2$), although not significant ($p > 0.05$). After inducing cLTP, the Shank3 structure size does not change in WT ($0.404 \pm 0.030 \mu\text{m}^2$; $p > 0.05$). We observed a very slight decrease in the S1510D phospho-mimic mutation ($0.469 \pm 0.038 \mu\text{m}^2$; $p > 0.05$). Interestingly, in the S1510A phospho-dead mutation the Shank3 structure size increased marginally ($0.512 \pm 0.038 \mu\text{m}^2$), although not significant compared to basal state ($p > 0.05$).

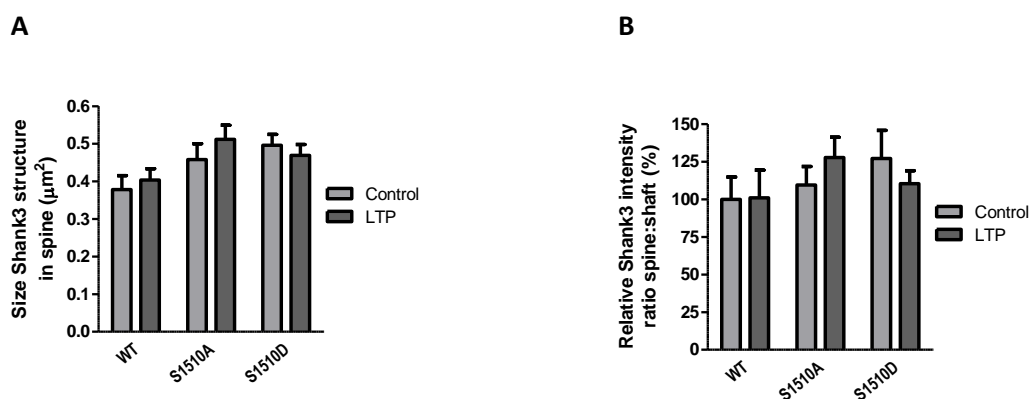


Figure 2: S1510 phosphorylation possibly affects Shank3 localization and size after cLTP

A: Quantification of Shank3 structure size (μm^2) for all conditions shown as mean + SEM. Number of neurons: WT ctrl n=9; WT LTP n=7; S1510A ctrl n=10; S1510A LTP n=10; S1510D ctrl n=6; S1510D LTP n=9

B: Quantification of relative intensity ratio spine:shaft for all conditions shown as mean + SEM. Number of neurons: WT ctrl n=7; WT LTP n=6; S1510A ctrl n=7; S1510A LTP n=7; S1510D ctrl n=6; S1510D LTP n=7

We also looked at the Shank3 intensity ratio spine:shaft, to see if the localization pattern of Shank3 is altered by the S1510 phosphorylation mutations (fig. 2B). In basal state, we did not observe a difference in relative spine:shaft ratio between the S1510A phospho-dead mutation ($109.6 \pm 12.3\%$) compared to WT ($100.0 \pm 14.9\%$; $p > 0.05$). In the S1510D phospho-mimic mutation, we observed a slight shift towards spine ($127.2\% \pm 18.7\%$), although not significantly different from WT ($p > 0.05$). Inducing cLTP did not change the Shank3 intensity in WT compared to basal state ($101.1 \pm 18.4\%$; $p > 0.05$). The S1510A phospho-dead mutation caused a small, not significant trend towards spine after inducing cLTP ($127.9 \pm 13.4\%$; $p > 0.05$), whereas the S1510D phospho-mimic mutation caused a small, not significant trending shift towards shaft compared to basal state ($110.4 \pm 8.7\%$; $p > 0.05$).

Despite the lack of significant changes in basal state nor after inducing cLTP, a small trend is observed where the mutations shift towards opposite directions after inducing cLTP. For the S1510A phospho-dead mutation, Shank3 structure size slightly increased and the intensity shifted towards spine. The S1510D phospho-mimic mutation showed a small decrease in size and an intensity shift towards shaft.

S1510 phosphorylation mutations do not affect extracellular GluA2 levels

It is known that LTP leads to exocytosis of AMPA receptors (AMPA receptors) (Kopec et al., 2006). Raynaud et al. (2013) show that Shank3 is involved in this AMPAR exocytosis. Therefore, we wanted to know if the S1510 phosphorylation could affect the AMPAR exocytosis after inducing cLTP. For this, we used an antibody that binds the extracellular part of GluA2, a subunit of the AMPAR, which thus labels the AMPARs in the membrane (fig 3A). Specifically GluA2 is chosen because the majority of AMPARs are heteromers consisting of either GluA1/GluA2 or GluA2/GluA3 (Wentholt et al., 1996), therefore GluA2 is present in the majority of AMPARs. We found that, despite some variance, the relative GluA2 intensity in the synaptic membrane in basal state does not significantly differ between EV ($150.3 \pm 39.85\%$), WT ($100.0 \pm 23.15\%$), S1510A phospho-dead mutation ($158.9 \pm 59.57\%$), or S1510D phospho-mimic mutation ($122.8 \pm 12.17\%$), shown in fig. 3C. After inducing cLTP, we observed a trend in increasing GluA2 intensity in EV ($184.7 \pm 61.35\%$), though not significant ($p > 0.05$; fig. 3C). These results after cLTP in the EV are significantly different from WT ($p < 0.05$; fig. 3C), where the relative intensity slightly decreased after inducing cLTP ($60.9 \pm 14.84\%$). A minor, not significant, decrease after cLTP is also seen in the S1510A phospho-dead mutation ($103.4 \pm 29.32\%$; $p > 0.05$; fig. 3C). There is no difference after inducing cLTP in the S1510D phospho-mimic mutation ($121.9 \pm 16.00\%$; $p > 0.05$; fig. 3C). Furthermore, we looked at the relative GluA2 level in the whole spine, so also the intracellular part. We used the same antibody but incubated it in a solution containing Triton-X, thereby perfusing the membrane (fig. 3B). As shown in fig. 3D, there is no significant difference in basal state between EV ($148.7 \pm 11.48\%$), WT ($100.0 \pm 12.44\%$), S1510A phospho-dead mutation ($124.2\% \pm 23.05\%$), or S1510D phospho-mimic mutation ($141.8 \pm 28.93\%$). After inducing cLTP, we observed a significant increase in GluA2 intensity in WT ($318.4 \pm 39.8\%$; $p < 0.05$). Even though we found this increase in WT, we did not observe a significant increase in EV ($161.9 \pm 39.80\%$; $p > 0.05$). In the S1510A phospho-dead mutation as well as the S1510D phospho-mimic mutation, there was also no significant difference after cLTP. If anything, there is a slight decrease in relative GluA2 intensity (resp. $72.2 \pm 60.09\%$ and $118.4 \pm 17.12\%$).

Altogether, this shows that overexpressing Shank3 WT causes a decrease in GluA2 intensity in the membrane and an increase in the spine after inducing cLTP. This effect, however, is not observed by the S1510A phospho-dead as well as the S1510D phospho-mimic mutation, which are both not significantly different from EV. This also shows no significant difference in GluA2 intensity levels between the S1510 phosphorylation mutations.

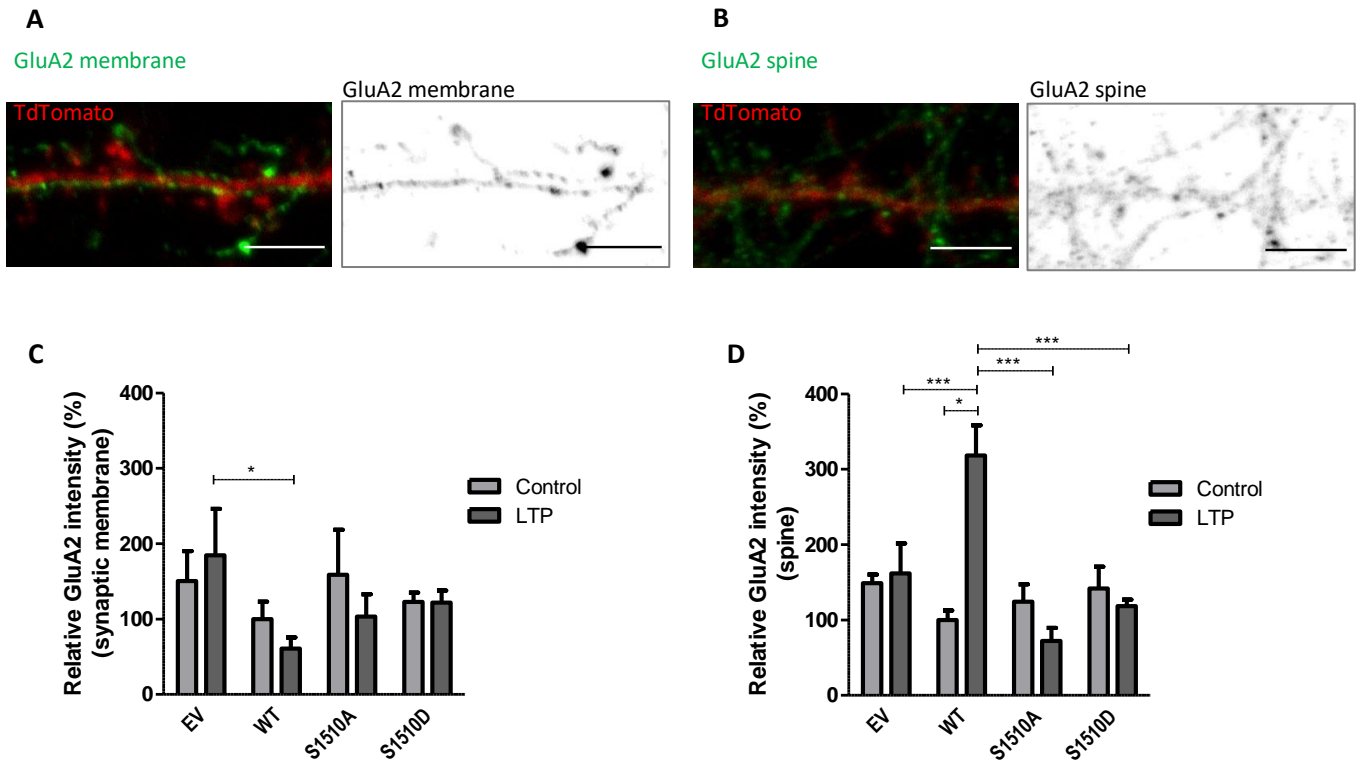


Figure 3: S1510 phosphorylation mutations do not affect GluA2 intensity levels

A: Neuron overexpressing Shank3 WT and tdTomato (red). Labeled for extracellular GluA2 (green). Scale bar: 5 μ m

B: Neuron overexpressing Shank3 WT and tdTomato (red). Labeled for extracellular GluA2 incubated in a solution containing Triton-X, (green). Scale bar: 5 μ m

C: Quantification of relative extracellular GluA2 levels for all conditions, shown as mean + SEM. Number of neurons: EV ctrl n=5; EV LTP n=4; WT ctrl n=4; WT LTP n=5; S1510A ctrl n=4; S1510A LTP n=4; S1510D ctrl n=5; S1510D LTP n=5

D: Quantification of relative GluA2 levels in the spine for all conditions, shown as mean + SEM. Number of neurons: EV ctrl n=5; EV LTP n=3; WT ctrl n=5; WT LTP n=3; S1510A ctrl n=4; S1510A LTP n=3; S1510D ctrl n=5; S1510D LTP n=3

S1510 mutations do not alter Shank3 interactions

Besides these neuronal characteristics visualized by confocal microscopy, we also examined if the S1510 phosphorylation mutations would alter Shank3 oligomerization or its interaction with Homer3, Cortactin, Rich2, or GKAP. We chose specifically for these proteins because Homer and Cortactin interact with the Proline rich domain of Shank3 (Naisbitt et al., 1999), which is close to S1510. GKAP is chosen because of its important function in anchoring NMDA receptors (Naisbitt et al., 1999), and Rich2 is chosen because the Shank3-Rich2 interaction is involved in AMPAR exocytosis after LTP (Raynaud et al., 2013).

We tested this with co-immunoprecipitation (co-IP). For this, we tagged Shank3 WT and the S1510 phosphorylation mutations with an HA-tag, and the interaction proteins with a Flag-tag. These constructs were co-transfected in HEK-293 cells, which were used to prepare lysates. HA-antibody was used for the immunoprecipitation, which thus precipitated the HA-Shank3 construct. The Flag-interaction protein is bound to that, and thus is also precipitated in the interaction complex. This was resolved by SDS-page, whereafter an HA-antibody was used to label the precipitated Shank3, and a Flag-antibody was used to label the fraction bound to HA-Shank3. Importantly, the Flag-tag itself did not interact with HA-Shank3 as is shown in supplementary figure 2B, where we used Flag-tagged UBE3A which does not interact with HA-Shank3.

We show that Shank3 indeed oligomerizes, as we co-transfected HA-Shank3 WT, S1510A, or S1510D phosphorylation mutations with Flag-Shank3 WT. We precipitated HA-tagged Shank3 constructs, and show that Flag-Shank3 is present in the bound fraction (fig. 4A). The S1510A phospho-dead mutation did not affect the efficiency of Shank3 oligomerization (109.8%), whereas the S1510D phospho-mimic mutation showed a

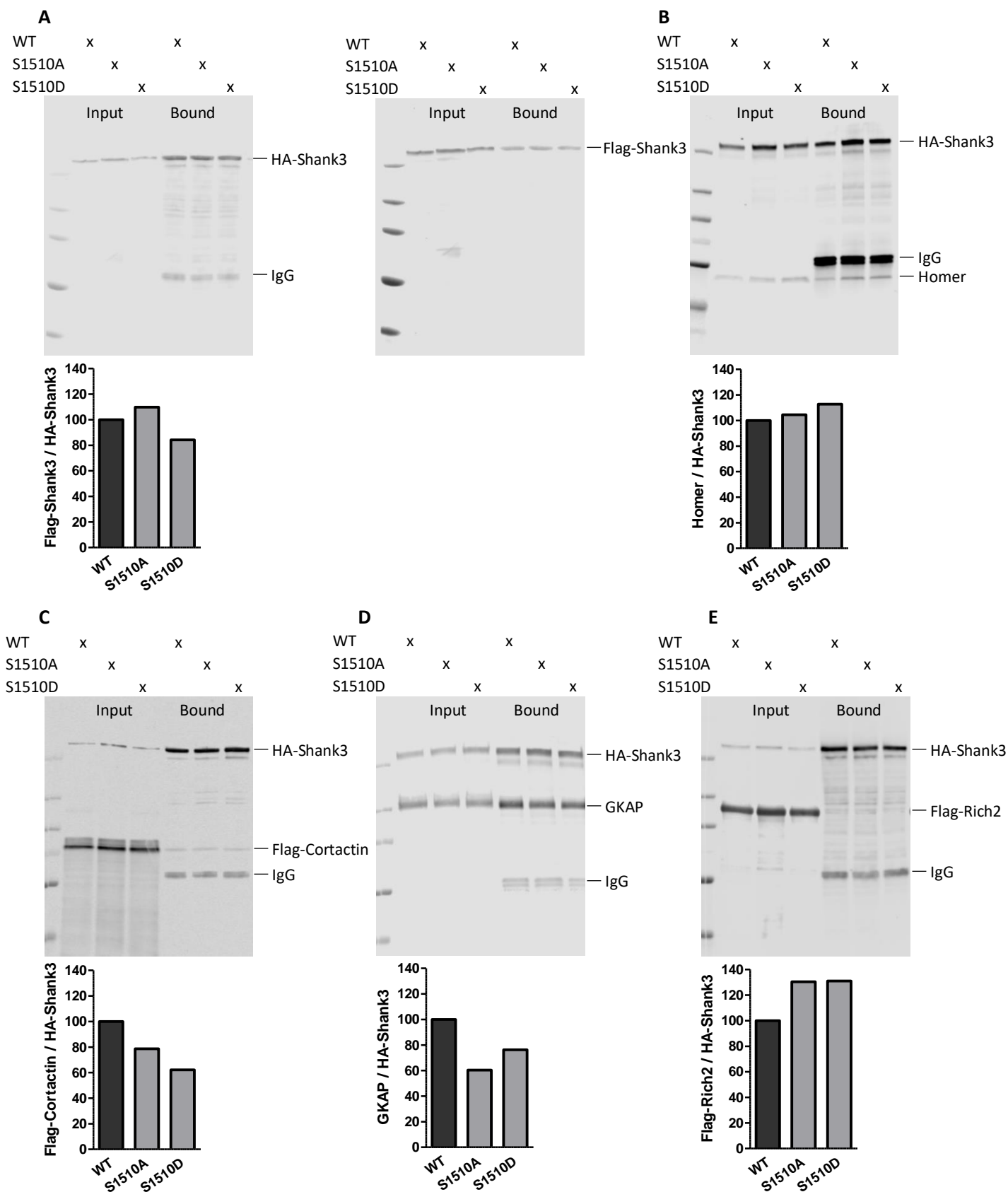


Figure 4. S1510 phosphorylation mutations possibly affect the interaction with Cortactin, Rich2, and GKAP

A-E: co-immunoprecipitation: HA-Shank3 was co-transfected in HEK-293T cells with Flag-Shank3 (A), Homer (B), Flag-Cortactin (C), GKAP (D), or Flag-Rich2 (E). Pulldown is done with anti-HA antibody, input and bound bands are shown. Quantifications are calculated by dividing the intensity of the bound interaction protein by bound HA-Shank3 intensity, which were plotted as percentage relative to WT. N=1 for all co-IPs.

minor decrease in oligomerization efficiency relative to Shank3 WT (84.2%). Next, we also show the Homer3 interaction with HA-Shank3 (fig. 4B). Both the S1510A phospho-dead and the S1510D phospho-mimic mutation show no change in interaction efficiency relative to WT (resp. 104.5% and 112.8%).

We show an interaction between HA-Shank3 and Flag-Cortactin (fig. 4C). The interaction efficiency decreased for both S1510 phosphorylation mutations relative to WT (S1510A: 78.6%; S1510D: 62.2%). This decrease in interaction efficiency is also found for the interaction between HA-Shank3 and GKAP. We confirm this interaction in figure 4D. Relative to WT, the S1510A phospho-dead mutation precipitated 60.5% GKAP. The S1510D phospho-mimic mutation precipitated 76.2% GKAP relative to WT. On the contrary, the interaction efficiency between HA-Shank3 and Flag-Rich2 is increased in both mutations. The interaction between HA-Shank3 and Flag-Rich2 is confirmed in figure 4E. The S1510A phospho-dead mutation precipitated relative 130.4% compared to WT, whereas the S1510D phospho-mimic mutation precipitated relative 131.1%. Complete SDS-page gels for all these co-IPs are shown in supplementary figure 2.

Altogether, this shows that Shank3 forms an interaction with all proteins tested, and that the S1510 phosphorylation mutations do not prevent this interaction. This also shows that the interaction with Homer3 was not affected by the S1510 phosphorylation mutations. Shank3 oligomerization is slightly decreased in the S1510D phospho-mimic mutation. A decreased interaction efficiency is also shown in Cortactin and GKAP, in contrast to the interaction efficiency in Rich2 which is increased relative to WT. Importantly, the interaction efficiency shifted in the same direction for the S1510A phospho-dead mutation as well as the S1510D phospho-mimic mutation for all these interaction proteins.

Discussion

Shank3 is an important scaffolding protein in the PSD where it interacts with multiple proteins and functions in various processes, among which connecting the PSD to the Actin cytoskeleton (Monteiro & Feng, 2017). In a recent phospho-proteomics study, Serine 1510 came forward as possibly an important phosphorylation site on Shank3, likely phosphorylated by CaMKII. The function of this phosphorylation site is unclear. By using an S1510A phospho-dead and an S1510D phospho-mimic mutation, we aimed to clarify this function with the research question “What is the effect of S1510 phosphorylation on Shank3 functioning?”. We found that both S1510 phosphorylation mutations do not show an effect on spine count nor on spine morphology in basal state and after inducing cLTP. S1510A phospho-dead mutations shows a slight increase in Shank3 structure size and localizes more in the spine after inducing cLTP. The S1510D phospho-mimic mutation, on the contrary, shows a small decrease in Shank3 structure size and localizes more in the shaft after inducing cLTP. The S1510 phosphorylation mutations do not show an effect on GluA2 levels in the membrane nor in the spine. Lastly, the S1510 phosphorylation mutations show some effect on interaction efficiency between Shank3 and Cortactin, Rich2, and GKAP, where both mutations show either an increased or decreased interaction efficiency compared to WT.

First, we looked at spine morphogenesis by analysing the number of spines and their morphology ratio mushroom:filopodium. For both the number of spines as well as the morphology ratio, there was no significant difference between EV and WT in basal state nor after inducing cLTP. This shows that overexpressing Shank3 did not affect the spine morphogenesis here, which is contradicting with other studies who show that overexpressing Shank3 increases the number of spines (Durand et al., 2012; Sala et al., 2001), and initiates spine maturation (Sala et al., 2001). Furthermore, we show that in basal state both S1510 phosphorylation mutations have a reduced number of spines. This is in agreement with Durand et al. (2012), who show that multiple other Shank3 mutations also have a decreased number of spines. Both S1510 phosphorylation mutations having this decreased number of spines, and the fact that other Shank3 mutations also show this, could imply that this might not be caused by the mimicking of S1510 phosphorylation. It might rather be a different, possibly more general aspect of Shank3 mutations. After inducing cLTP, both S1510 phosphorylation

mutations showed an increase in number of spines, a known effect of LTP (Engert & Bonhoeffer, 1999; Maletic-Savatic et al., 1999). Against our expectations, this effect is not observed in EV and WT. Another known effect of LTP is an increase in the number of mushroom spines (Murakoshi & Yasuda, 2012), however this effect is not observed at all. This indicates that the protocol to induce cLTP used here might not be very efficient. Repeating these experiments with a different LTP protocol, for instance by adding a Ca²⁺ ionophore which activates CaMKII, or by applying Glutamate to activate receptors (Molnár, 2011), would be useful to confirm the results from this project.

Next, we looked at Shank3 localization in spines. We analysed the size of Shank3 structures in spines and the Shank3 intensity ratio spine:shaft. The results show opposite trends for the S1510 phosphorylation mutations after inducing cLTP. The S1510A phospho-dead mutation has an increased Shank3 structure size and localizes more in the spine after inducing cLTP. The S1510D phospho-mimic mutation, however, has a decreased Shank3 structure size and localizes more in the shaft after inducing cLTP. Despite that these results are not significant, they do act in opposite directions. This could indicate that S1510 phosphorylation affects Shank3 recruitment in the spine after inducing cLTP. Other studies also show similar results on Shank3 recruitment. For instance, Jeong et al. (2021) also show an increase in Shank3 structure size in a phospho-dead mutant (S782A), although this is a different phosphorylation site (S782). Tao-Cheng et al. (2014) show that CaMKII is involved in Shank3 accumulation at the PSD upon neuronal activation. This is opposite from our results, as they show an increase in Shank3 intensity when CaMKII is activated, whereas we show a decrease in Shank3 intensity in the PSD in the S1510D phospho-mimic mutation. However, it is known that phosphorylation by CaMKII also can have an inhibiting effect, rather than activating (Song et al., 2010), which could be true for S1510 phosphorylation. Taken all these results into account, it is known that CaMKII is involved in Shank3 recruitment upon neuronal activation. Based on our data, S1510 phosphorylation possibly also has an effect on this. In order to get to know the exact effect of S1510 phosphorylation, more experiments should be performed. This can be done by repeating these experiments and combining it with live-cell imaging, to visualize the recruitment of Shank3 after inducing cLTP in the S1510 phosphorylation mutations.

Furthermore, we looked at the GluA2 levels in the postsynaptic membrane and in the spine. We show that, after inducing cLTP, GluA2 intensity levels in the spine increase strongly in Shank3 WT. In the postsynaptic membrane, the intensity levels strongly decrease. This is not as expected, as Tanaka & Hirano (2012) show that GluA2 is exocytosed after LTP, and thus an increase in the membrane was expected. It could indicate that overexpressing Shank3 causes an artefact in GluA2 exocytosis which leads to GluA2 accumulation in the spine. It is known that Shank3 functions indirectly in AMPAR exocytosis after LTP via its interaction with Rich2 (Raynaud et al., 2013), and it is also known that Shank3 directly interacts with the GluA1 subunit of AMPARs (Uchino et al., 2006). Therefore, there is a possibility that overexpression of Shank3 affects the AMPAR trafficking or exocytosis, although this has not been reported before. Also, we do not notice this effect in both S1510 phosphorylation mutations, which also overexpress Shank3. This weakens the hypothesis of Shank3 overexpression interfering with GluA2 trafficking or exocytosis, and could indicate an experimental artefact. Additionally, we show no significant contrast in GluA2 intensity levels in either S1510A phospho-dead or S1510D phospho-mimic mutation in the spine nor in the membrane after inducing cLTP. Based on the data, it is not likely that GluA2 trafficking after LTP is affected by S1510 phosphorylation.

Lastly, we looked at the effect of S1510 phosphorylation on interaction efficiency between Shank3 and other proteins. Shank3 phosphorylation affecting an interaction has been shown before, for instance for Abi1 (Perfitt, Stauffer, et al., 2020). In preliminary experiments using a co-immunoprecipitation, we show that the interaction between HA-Shank3 and Flag-Cortactin, GKAP, and Flag-Rich2 are possibly affected. For GKAP, we show an increased interaction efficiency compared to WT for both S1510 phosphorylation mutations. This is opposite from an earlier study from Jeong et al. (2021), who show that a different Shank3 phosphorylation site (S782) did not affect the interaction between Shank3 and myc-GKAP. However, it is very well possible that S782 phosphorylation does not affect the interaction between Shank3 and GKAP, whereas S1510 phosphorylation does. The interaction between HA-Shank3 and Flag-Rich2 is increased in both S1510

phosphorylation mutations. Raynaud et al. (2013) show that a decreased interaction efficiency decreases the levels of exocytosed AMPARs after LTP. This suggests that an increased interaction efficiency could increase the exocytosis of AMPARs. However, this is not automatically true, the interaction efficiency could be increased without an increased effect on AMPAR exocytosis. This is also what we show in the GluA2 intensity levels. Furthermore, we show that the interaction between HA-Shank3 and Flag-Cortactin is also decreased in both S1510 phosphorylation mutations. It is known that a loss of interaction between Shank3 and Cortactin causes a decrease of Cortactin levels in the spine (MacGillavry et al., 2016). Cortactin has an important function in Actin spine dynamics, where it regulates stabilization of F-actin (Hering & Sheng, 2003). It also functions in the dynamics of spine morphology, where a loss of Shank3-Cortactin interaction leads to a decrease in spine morphological changes (MacGillavry et al., 2016). This could explain why we did observe an increased number of spines after inducing cLTP, but not a shift towards mushroom in the spine morphology ratio for both S1510 phosphorylation mutations. To test if the decreased interaction efficiency indeed causes this, the experiment with cultured neurons should be repeated. Additionally to the S1510 mutation constructs, neurons should be transfected with a Cortactin construct lacking the Shank3 binding site. This would provide information about the localization of Cortactin and the colocalization between Shank3 and Cortactin. It would also show the effect of the interaction between Shank3 and Cortactin on spine morphology after inducing LTP in the S1510 phosphorylation mutations.

Taken altogether, we show that of all functions we tested here, S1510 phosphorylation is only possibly a regulator of Shank3 recruitment in the PSD after inducing cLTP. We also show that S1510 phosphorylation possibly affects some interactions. Interestingly, these interactions and also the effects on number of spines are similar for both S1510 mutations, being both either increased or decreased compared to WT. This might indicate that the S1510A and S1510D mutations possibly do not mimic the phosphorylation situations, but rather have a different effect on Shank3. This could be a change in folding, for instance, which can make the access to an interaction site less accessible. To find out if this is true, mutations at S1510 with other amino acids can be designed, to see if these cause similar results.

In this project, we aimed to find out what the effect of S1510 phosphorylation is on Shank3 functioning. Despite this phosphorylation site came forward as possibly important for Shank3 regulation, we do not find big differences between the S1510A phospho-dead and S1510D phospho-mimic mutation. This implies that S1510 might not be as important for the regulation of Shank3 as previously thought.

Material and Methods

DNA constructs

The S1510 mutations were cloned in a vector containing a tdTomato gene under a different promoter and with multiple cloning sites. This vector without an inserted gene is used as a control in multiple experiments (empty vector, EV). Mutations in Shank3 were introduced using PCR with primers shown in table 1. The HA tag and Flag-tag were cloned in the vector with the protein of interest using EcoRI-HF (New England Biolabs, R3101) and Ascl (New England Biolabs, R0558) restriction enzymes in combination with sticky-end primers (table 1).

Table 1. Primers

Usage	Primer forward	Primer reverse
Mutagenesis S1510A (PCR)	tagtctaagcttCACAGCGCTTCTGGTAG ATG	CTGGTTCCTCCCCCAAgccGCGTGTGTCTT TATTC
Mutagenesis S1510D (PCR)	tagtctaagcttCACAGCGCTTCTGGTAG ATG	CTGGTTCCTCCCCCAAtcGCGTGTGTCTTT ATTC
3x HA-tag (cloning)	AATTCACCATGTACCCATACGATGTTCCAG ATTACGCTTATCCATATGATGTTCCAGATT ATGCTTACCCATACGATGTTCCAGATTACG CTggcagcgccGGG	CGCGCCggcgctgccAGCGTAATCTGGAACATCG TATGGGTAAGCATAATCTGGAACATCATATGGA TAAGCGTAATCTGGAACATCGTATGGGTACATG GTG
3x Flag-tag (cloning)	AATTCaccatggactacaaagaccatgacggtgatta taaagatcatgacatcgattacaaggatgacgatgaca agggcagcgccGG	CGCGCCggcgctgcccttgtcatgctcatccttgaatcgat gtcatgactttataatcaccgtcatggtcttttagtccatggt G

Co-immunoprecipitation

HEK293T cells were grown in DMEM complete, consisting of DMEM (Gibco) supplemented with Fetal Bovine Serum (FBS, 10%), and penicillin/streptomycin (p/s, 1%). For the co-immunoprecipitation (co-IP), a 10 cm dish with HEK cells was transfected by mixing 20 µg DNA with 1 mL serum-free DMEM. Polyethylenimine (PEI) was then added to this DNA mixture in the ratio PEI:DNA 3 µL:1µg, which was incubated for 15 minutes at room temperature (RT) and then added to the HEK-cells in fresh DMEM complete. The medium was refreshed after 5-7 hours incubation at 37 °C and 5% CO₂ with DMEM complete. After the medium refresh, cells were incubated at 37 °C and 5% CO₂ until harvesting.

Co-IP was performed by harvesting the transfected HEK cells two days post transfection. Cell lysates were made in lysis buffer consisting of Tris (20 mM), NaCl (150 mM), NP40 (1%), protease inhibitor (1:50), and phosphatase inhibitor (1:100). 600 µg of protein was diluted in 800 µL lysis buffer, of which 32,5 µL was set aside as input. The remaining sample was incubated with Protein A Sepharose beads (GE Healthcare) at 4 °C for 1 hour. Samples were spun down and the supernatant was used to incubate with anti-HA rabbit antibody (1:140) over night (o/n) at 4 °C. The next day, samples were incubated with Protein A Sepharose beads for 1 hour at 4 °C. Thereafter, samples were spun down, and the pellet is washed 3 times with lysis buffer. 32,5 µL of the supernatant is set aside as unbound. Input and unbound samples were supplemented with XT sample buffer (12,5 µL; Bio-rad) and dithiothreitol (5 µL, Sigma-Aldrich). The bound sample was supplemented with XT sample buffer (12,5 µL; Bio-rad), dithiothreitol (2 µL, Sigma-Aldrich) and 13 µL Laemmli buffer (0.1M Tris-HCl, 4% SDS). All samples were boiled at 95 °C for 5 min, whereafter 20 µL per sample was loaded on an SDS-page gel. The gel was transferred to a nitrocellulose membrane (Biorad). This membrane was labelled with either anti-Flag, anti-Homer, or anti-GKAP antibody diluted in 2% milk o/n at 4 °C, washed with 2% milk two times 10 minutes at RT, then labelled with Licor Rabbit-red or Mouse-green for 1h at RT. The membrane is then washed three times with TBS-T (10 mM TrisHCl pH 8.0, 150 mM NaCl, 0.1% Tween), and two times with TBS (10 mM TrisHCl pH 8.0, 150 mM NaCl) 10 minutes at RT, and then developed with a Licor Odyssey. Thereafter, the membrane is labelled with anti-HA antibody, also diluted in 2% milk o/n at 4 °C. All

washing, labelling, and developing steps are repeated. All antibodies and their concentrations are shown in table 2.

Neurons

Primary hippocampal mouse neurons are cultured as described earlier (Goslin & Banker, 1991). Briefly, neurons are cultured from E16.5 FvB/NHsD wild-type mouse hippocampi and plated on coverslips (\varnothing 18 mm) coated with poly-D-lysine (Invitrogen), with a density of 1×10^6 neurons/coverslip. Neurons are grown in 1 ml Neurobasal (NB) medium (Gibco), supplemented with B27 (2%), penicillin/streptomycin (p/s) (1%) and 1% glutamax (Invitrogen), at 37 °C and 5% CO₂ until transfection.

Neurons were transfected at days in vitro (DIV) 10 or 11 with either an empty vector (EV) (1.8 μ g DNA per coverslip) or a vector with one of the Shank3 constructs mentioned earlier (3 μ g DNA per coverslip). DNA was mixed with 200 μ L unsupplemented NB per coverslip. 3,33 μ L Lipofectamine 2000 (Invitrogen) was added and incubated for 5 minutes. The coverslips were shifted from their original medium to fresh NB, supplemented with glutamine (0.25%), to where the DNA mixture was added. This was incubated for 45-60 min at 37 °C and 5% CO₂. After incubation in the DNA mixture, the coverslips were shifted back to their original medium and incubated for 4-5 days until treatment and fixation.

Neurons were treated for LTP or control and thereafter fixated at DIV 15. Before inducing LTP, neuronal activity of both the LTP and control group was stopped by incubating the coverslips for 30 min at 37 °C and 5% CO₂ in 5K tyrode's consisting of 150 mM NaCl, 5 mM KCl, 2 mM CaCl₂, 2 mM MgCl₂, 10 mM glucose, and 10 mM HEPES. This 5K tyrode's is supplemented with NBQX (50 μ M), TTX (1 μ M), and AP5 (10 μ M) to inhibit neuronal activity. Thereafter, LTP was induced by incubating the coverslips for five minutes at 37 °C and 5% CO₂ in 5K tyrode's without magnesium and increased calcium concentration (150 mM NaCl, 5 mM KCl, 3 mM CaCl₂, 10 mM glucose, 10 mM HEPES), and supplemented with glycine (200 μ M) and bicuculline dissolved in DMSO (20 μ M). For the basal group, the neuronal activity was inhibited by incubating the coverslips for five minutes at 37 °C and 5% CO₂ in fresh 5K tyrode's supplemented with NBQX (50 μ M), TTX (1 μ M), AP5 (10 μ M), and DMSO (20 μ M), to increase the difference between control and LTP. After 5 minutes of incubation, coverslips of both the control and LTP group were shifted to their original supplemented NB medium, in which they recovered for 30 min at 37 °C and 5% CO₂. After 30 minutes recovery, neurons were fixed using 4% PFA 4% sucrose, incubating for 10 min at room temperature (RT).

Neurons were then washed three times with dPBS (Lonza) for 5-10 minutes at RT. Thereafter, neurons were labelled. Antibodies were diluted in GDB (5% Gelatine 2%, 0,003% Triton X, 3.33 mM Phosphate buffer, 333 mM NaCl), except the GluA2 extracellular antibody and its secondary antibody, which were diluted in dPBS. Primary antibodies were o/n at 4 °C. The next morning, coverslips were washed 3 times with \sim 750 μ L dPBS 5-10 minutes, whereafter secondary antibodies were incubated for 1h at RT. After 1h of incubation, neurons were washed three times with 750 μ L dPBS 5-10 minutes and then mounted in 8 μ L Mowiol. All antibodies and concentrations are shown in table 2.

Imaging + analysis

Images were taken with a ZEISS confocal microscope, with a 20x air objective or 63x oil objective. Z-stacks were taken with steps of 0.77 μ m, 5-7 stacks per image. Analysis was performed in either ImageJ (Schindelin et al., 2012), or ICY (De Chaumont et al., 2012), on a maximum Z-stack projection.

To quantify the number of spines, 4-5 regions of interest (ROIs) of 20 in length μ m each were drawn over secondary and/or tertiary dendrites in a neuron. In these ROIs, all spines were counted, and the average per neuron was calculated and plotted. These spines in the ROIs were also quantified for their morphology. Spine morphology was determined by measuring the width of the spine head, and dividing this by the length of the spine neck from the top of the spine to the edge of the dendrite. Spines with a ratio higher than 0.5 were

considered mushroom, and spines with a ratio lower than 0.5 were considered filopodium. The ratio mushroom:filopodium was calculated per neuron as percentages and plotted.

The size of Shank3 structures was calculated by creating a binary image using the point detector plugin in ICY with a threshold of 70%. This binary image was loaded in ImageJ, where the size of Shank3 structures was quantified using ImageJ measure particles. Only the Shank3 structures of the spines counted above were used for the analysis and plotted.

To analyse intensity of Shank3 spine:shaft ratio, ROIs were drawn around the borders of a Shank3 spine structure, in the shaft closest to the spine, and also an ROI in the background close by. Integrated density, mean fluorescence, and area were determined for all these ROIs by using “measure particles” in ImageJ. Corrected total fluorescence (CTF) was then calculated as follows: Integrated density – (area ROI*mean fluorescence background). The CTF of spine and related shaft were used to calculate the ratio spine:shaft. These values were averaged per neuron and normalized to wildtype.

The intensity of GluA2 was calculated similarly, except there was no shaft intensity analysed. As the laser settings were kept similar for all images, CTF values itself were used to average per neuron and normalize to wildtype.

Analysis of co-IP membranes was performed using Image Studio Lite 4.2. Intensity levels were determined by placing ROIs over the bands of interest. The ratio of precipitated protein was calculated by dividing the value of bound interaction protein by the value of bound pulled down protein. These values were normalized to the wildtype.

Table 2: antibodies used and their concentration

Antibody	Host animal	Company	Dilution in neurons	Dilution in western blots / co-IP
anti-Shank3	Mouse	Santa Cruz (377088)	1:500	
anti-Synapsin 1	Rabbit	Merck Millipore (AB1543P)	1:200	
anti-GluA2 extracellular	Rabbit	Alomone (AGC-005)	1:200	
anti-HA	Rabbit	Cell signaling tech (3724)		1:1000
anti-Flag	Mouse	Proteintech (F1804)		1:3000
anti-Homer	Rabbit			1:4000
anti-GKAP	Mouse	Novus Biologicals (S127-31)		1:1000
Alexa-488 anti-rabbit		Jackson Immuno Research	1:200	
Alexa-488 anti-mouse		Jackson Immuno Research	1:200	
Alexa-647 anti-rabbit		Jackson Immuno Research	1:200	
Licor Mouse-Green		Licor		1:15000
Licor Rabbit-red		Licor		1:15000

Statistics

In table 3, all statistical tests are shown including their P-value

Table 3: statistical tests

Figure	Statistical test	Condition	p-value
1I	Two-way Anova with Bonferroni posthoc test	Control vs LTP EV WT S1510A S1510D Control EV vs WT EV vs S1510A EV vs S1510D WT vs S1510A WT vs S1510D S1510A vs S1510D LTP EV vs WT EV vs S1510A EV vs S1510D WT vs S1510A WT vs S1510D S1510A vs S1510D	p>0.05 (ns) p>0.05 (ns) p<0.05 (*) p<0.05 (*) p>0.05 (ns) p>0.05 (ns) p>0.05 (ns) p<0.05 (*) p>0.05 (ns) p>0.05 (ns) p>0.05 (ns) p>0.05 (ns) p>0.05 (ns) p>0.05 (ns) p>0.05 (ns) p>0.05 (ns)
1J	Two-way Anova with Bonferroni posthoc test	Control vs LTP EV WT S1510A S1510D Control EV vs WT EV vs S1510A EV vs S1510D WT vs S1510A WT vs S1510D S1510A vs S1510D LTP EV vs WT EV vs S1510A EV vs S1510D WT vs S1510A WT vs S1510D S1510A vs S1510D	p>0.05 (ns) p>0.05 (ns) p>0.05 (ns) p>0.05 (ns) p>0.05 (ns) p>0.05 (ns) p>0.05 (ns) p>0.05 (ns) p>0.05 (ns) p>0.05 (ns) p>0.05 (ns) p>0.05 (ns) p<0.01 (**) p<0.001 (***) p>0.05 (ns) p<0.01 (**) p>0.05 (ns)
2A	Two-way Anova with Bonferroni posthoc test	Control vs LTP WT S1510A S1510D Control WT vs S1510A WT vs S1510D S1510A vs S1510D LTP WT vs S1510A WT vs S1510D	p>0.05 (ns) p>0.05 (ns) p>0.05 (ns) p>0.05 (ns) p>0.05 (ns) p>0.05 (ns) p>0.05 (ns) p>0.05 (ns)

		S1510A vs S1510D	p>0.05 (ns)
2B	Two-way Anova with Bonferroni posthoc test	Control vs LTP WT S1510A S1510D Control WT vs S1510A WT vs S1510D S1510A vs S1510D LTP WT vs S1510A WT vs S1510D S1510A vs S1510D	p>0.05 (ns) p>0.05 (ns) p>0.05 (ns) p>0.05 (ns) p>0.05 (ns) p>0.05 (ns) p>0.05 (ns) p>0.05 (ns) p>0.05 (ns)
3C	Two-way Anova with Bonferroni posthoc test	Control vs LTP EV WT S1510A S1510D Control EV vs WT EV vs S1510A EV vs S1510D WT vs S1510A WT vs S1510D S1510A vs S1510D LTP EV vs WT EV vs S1510A EV vs S1510D WT vs S1510A WT vs S1510D S1510A vs S1510D	p>0.05 (ns) p>0.05 (ns) p>0.05 (ns) p>0.05 (ns) p>0.05 (ns) p>0.05 (ns) p>0.05 (ns) p>0.05 (ns) p>0.05 (ns) p>0.05 (ns) p>0.05 (ns) p<0.05 (*) p>0.05 (ns) p>0.05 (ns) p>0.05 (ns) p>0.05 (ns) p>0.05 (ns)
3D	Two-way Anova with Bonferroni posthoc test	Control vs LTP EV WT S1510A S1510D Control EV vs WT EV vs S1510A EV vs S1510D WT vs S1510A WT vs S1510D S1510A vs S1510D LTP EV vs WT EV vs S1510A EV vs S1510D WT vs S1510A WT vs S1510D S1510A vs S1510D	p>0.05 (ns) p<0.001 (***) p>0.05 (ns) p>0.05 (ns) p>0.05 (ns) p>0.05 (ns) p>0.05 (ns) p>0.05 (ns) p>0.05 (ns) p>0.05 (ns) p>0.05 (ns) p<0.001 (***) p>0.05 (ns) p>0.05 (ns) p<0.001 (***) p<0.001 (***) p>0.05 (ns)

Supplementary figures

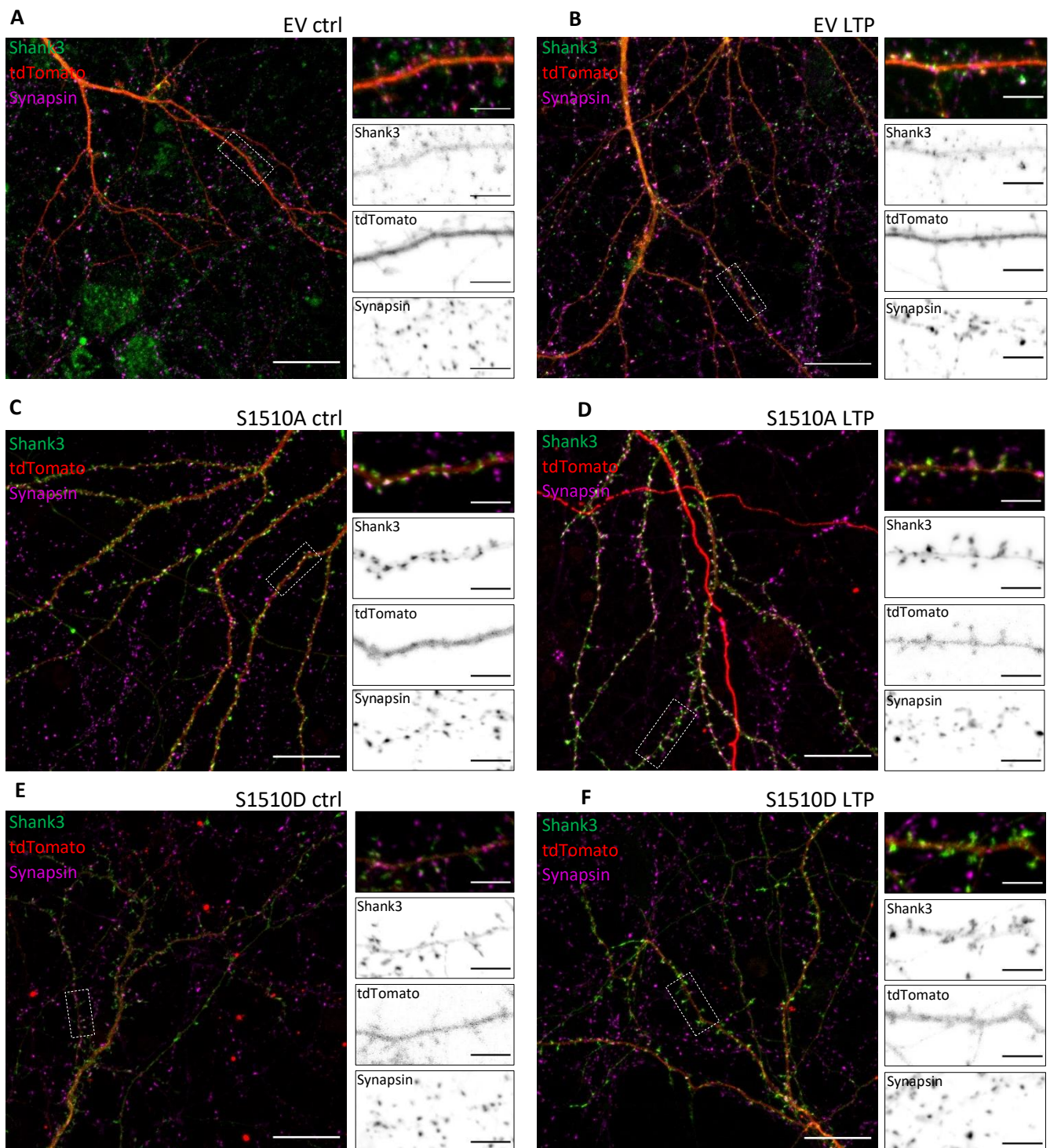


Figure S1. Example Images of all conditions

A-B: Neuron expressing EV construct with tdTomato (red), stained for Shank3 (green), and Synapsin (magenta). Dotted rectangle represents the zoom in of the dendrite on the right, corresponding to the dendrites in fig. 1. Scale bar 20 μm for the whole neuron, 5 μm for the zoomin

C-F: Neuron expressing a Shank3 construct (green) in combination with tdTomato (red), stained for Synapsin (magenta). Dotted rectangle represents the zoom in of the dendrite on the right, corresponding to the dendrites in fig. 1. Scale bar 20 μm for the whole neuron, 5 μm for the zoomin

Neurons expressing either EV or an S1510 phosphorylation mutation, also expressing tdTomato vector (red). Labelled for Shank3 (green) and Synapsin (magenta). Dotted rectangles represent zoomin at the right. Scale bar: neuron 20 μm ; zoomin 5 μm .

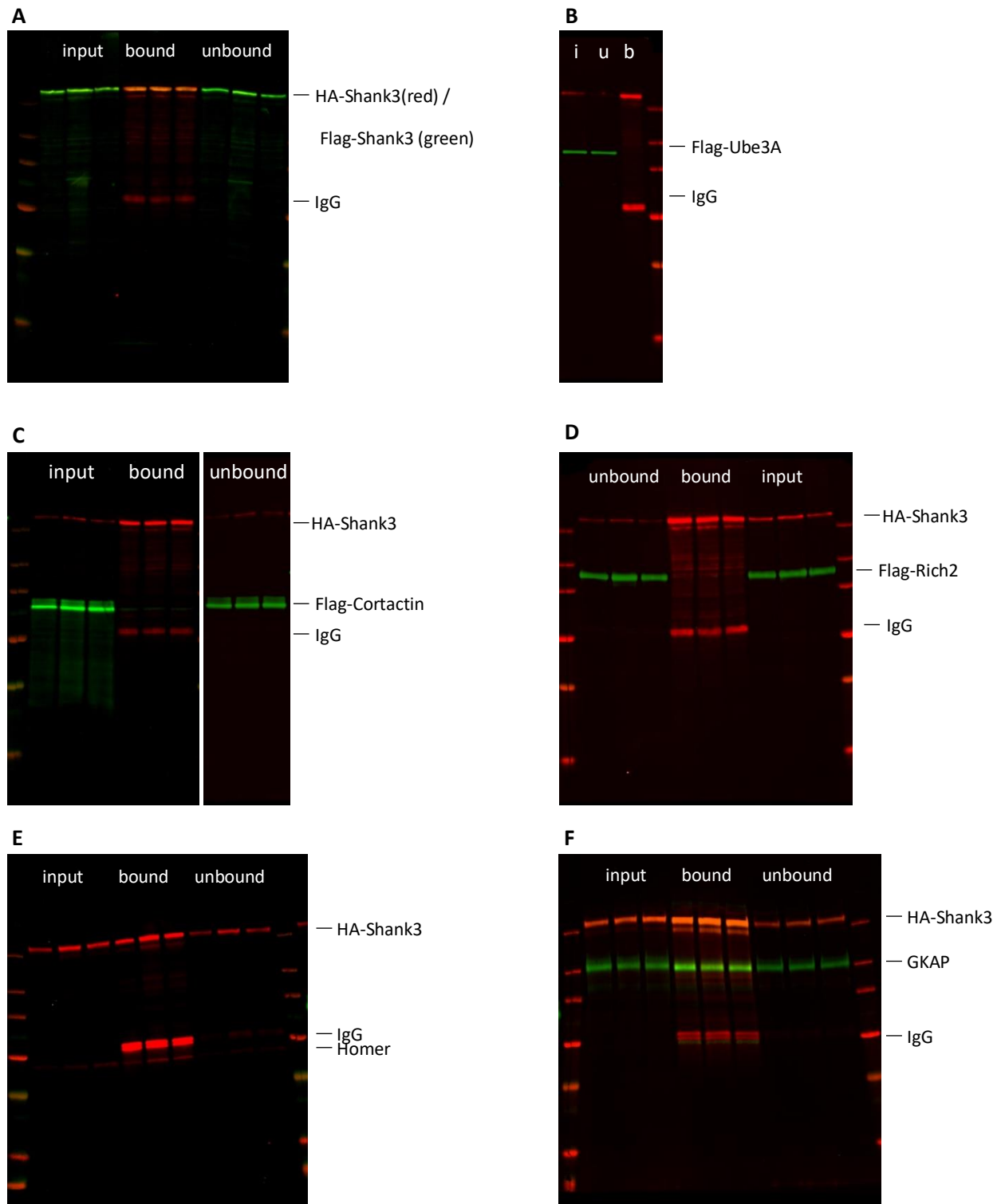


Figure S2. SDS-page gels for the co-immunoprecipitations from figure 3
Whole gels corresponding to the gels showed in figure 3, including the unbound fraction.

References

- Boeckers, T. M. (2006). The postsynaptic density. In *Cell and Tissue Research* (Vol. 326, Issue 2, pp. 409–422). Springer. <https://doi.org/10.1007/s00441-006-0274-5>
- Bozdagi, O., Sakurai, T., Papapetrou, D., Wang, X., Dickstein, D. L., Takahashi, N., Kajiwara, Y., Yang, M., Katz, A. M., Scattoni, M., Harris, M. J., Saxena, R., Silverman, J. L., Crawley, J. N., Zhou, Q., Hof, P. R., & Buxbaum, J. D. (2010). Haploinsufficiency of the autism-associated Shank3 gene leads to deficits in synaptic function, social interaction, and social communication. *Molecular Autism*, 1(1). <https://doi.org/10.1186/2040-2392-1-15>
- Citri, A., & Malenka, R. C. (2008). Synaptic plasticity: Multiple forms, functions, and mechanisms. In *Neuropsychopharmacology* (Vol. 33, Issue 1, pp. 18–41). <https://doi.org/10.1038/sj.npp.1301559>
- De Chaumont, F., Dallongeville, S., Chenouard, N., Hervé, N., Pop, S., Provoost, T., Meas-Yedid, V., Pankajakshan, P., Lecomte, T., Le Montagner, Y., Lagache, T., Dufour, A., & Olivo-Marin, J. C. (2012). Icy: An open bioimage informatics platform for extended reproducible research. In *Nature Methods* (Vol. 9, Issue 7, pp. 690–696). Nature Publishing Group. <https://doi.org/10.1038/nmeth.2075>
- Durand, C. M., Perroy, J., Loll, F., Perrais, D., Fagni, L., Bourgeron, T., Montcouquiol, M., & Sans, N. (2012). SHANK3 mutations identified in autism lead to modification of dendritic spine morphology via an actin-dependent mechanism. *Molecular Psychiatry*, 17(1), 71. <https://doi.org/10.1038/MP.2011.57>
- Engert, F., & Bonhoeffer, T. (1999). Dendritic spine changes associated with hippocampal long-term synaptic plasticity. *Nature* 1999 399:6731, 399(6731), 66–70. <https://doi.org/10.1038/19978>
- Goslin, K., & Banker, G. (1991). *Culturing Nerve Cells*. MIT Press: Cambridge. <https://mitpress.mit.edu/books/culturing-nerve-cells>
- Hering, H., & Sheng, M. (2003). Activity-Dependent Redistribution and Essential Role of Cortactin in Dendritic Spine Morphogenesis. *Journal of Neuroscience*, 23(37), 11759–11769. <https://doi.org/10.1523/jneurosci.23-37-11759.2003>
- Herring, B. E., & Nicoll, R. A. (2016). Long-Term Potentiation: From CaMKII to AMPA Receptor Trafficking. In *Annual Review of Physiology* (Vol. 78, pp. 351–365). <https://doi.org/10.1146/annurev-physiol-021014-071753>
- Jeong, J., Li, Y., & Roche, K. W. (2021). CaMKII Phosphorylation Regulates Synaptic Enrichment of Shank3. *ENeuro*, 8(3), ENEURO.0481-20.2021. <https://doi.org/10.1523/eneuro.0481-20.2021>
- Kool, M. J., Onori, M. P., Borgesius, N. Z., Van De Bree, J. E., Elgersma-Hooisma, M., Nio, E., Bezstarosti, K., Buitendijk, G. H. S., Jolfaei, M. A., Demmers, J. A. A., Elgersma, Y., & Van Woerden, G. M. (2019). CAMK2-dependent signaling in neurons is essential for survival. *Journal of Neuroscience*, 39(28), 5424–5439. <https://doi.org/10.1523/JNEUROSCI.1341-18.2019>
- Kopec, C. D., Li, B., Wei, W., Boehm, J., & Malinow, R. (2006). Glutamate receptor exocytosis and spine enlargement during chemically induced long-term potentiation. *Journal of Neuroscience*, 26(7), 2000–2009. <https://doi.org/10.1523/JNEUROSCI.3918-05.2006>
- Kouser, M., Speed, H. E., Dewey, C. M., Reimers, J. M., Widman, A. J., Gupta, N., Liu, S., Jaramillo, T. C., Bangash, M., Xiao, B., Worley, P. F., & Powell, C. M. (2013). Loss of predominant shank3 isoforms results in hippocampus-dependent impairments in behavior and synaptic transmission. *Journal of Neuroscience*, 33(47), 18448–18468. <https://doi.org/10.1523/JNEUROSCI.3017-13.2013>
- Lisman, J., Yasuda, R., & Raghavachari, S. (2012). Mechanisms of CaMKII action in long-term potentiation. In *Nature Reviews Neuroscience* (Vol. 13, Issue 3, pp. 169–182). Nature Publishing Group. <https://doi.org/10.1038/nrn3192>
- MacGillavry, H. D., Kerr, J. M., Kassner, J., Frost, N. A., & Blanpied, T. A. (2016). Shank-cortactin interactions control actin dynamics to maintain flexibility of neuronal spines and synapses. *European Journal of Neuroscience*, 43(2), 179–193. <https://doi.org/10.1111/ejn.13129>
- Maletic-Savatic, M., Malinow, R., & Svoboda, K. (1999). Rapid dendritic morphogenesis in CA1 hippocampal dendrites induced by synaptic activity. *Science*, 283(5409), 1923–1927. <https://doi.org/10.1126/science.283.5409.1923>
- Molnár, E. (2011). Long-term potentiation in cultured hippocampal neurons. *Seminars in Cell & Developmental Biology*, 22, 506–513. <https://doi.org/10.1016/j.semcd.2011.07.017>

- Monteiro, P., & Feng, G. (2017). SHANK proteins: Roles at the synapse and in autism spectrum disorder. In *Nature Reviews Neuroscience* (Vol. 18, Issue 3, pp. 147–157). Nature Publishing Group. <https://doi.org/10.1038/nrn.2016.183>
- Murakoshi, H., & Yasuda, R. (2012). Postsynaptic signaling during plasticity of dendritic spines. In *Trends in Neurosciences* (Vol. 35, Issue 2, pp. 135–143). <https://doi.org/10.1016/j.tins.2011.12.002>
- Naisbitt, S., Eunjoon, K., Tu, J. C., Xiao, B., Sala, C., Valtschanoff, J., Weinberg, R. J., Worley, P. F., & Sheng, M. (1999). Shank, a novel family of postsynaptic density proteins that binds to the NMDA receptor/PSD-95/GKAP complex and cortactin. *Neuron*, 23(3), 569–582. [https://doi.org/10.1016/S0896-6273\(00\)80809-0](https://doi.org/10.1016/S0896-6273(00)80809-0)
- Perfitt, T. L., Stauffer, P. E., Spiess, K. L., & Colbran, R. J. (2020). CaMKII α phosphorylation of Shank3 modulates ABI1-Shank3 interaction. *Biochemical and Biophysical Research Communications*, 524(1), 262–267. <https://doi.org/10.1016/j.bbrc.2020.01.089>
- Perfitt, T. L., Wang, X., Dickerson, M. T., Stephenson, J. R., Nakagawa, T., Jacobson, D. A., & Colbran, R. J. (2020). Neuronal L-type calcium channel signaling to the nucleus requires a novel CaMKII α -SHANK3 interaction. *Journal of Neuroscience*, 40(10), 2000–2014. <https://doi.org/10.1523/JNEUROSCI.0893-19.2020>
- Raynaud, F., Janossy, A., Dahl, J., Bertaso, F., Perroy, J., Varrault, A., Vidal, M., Worley, P. F., Boeckers, T. M., Bockaert, J., Marin, P., Fagni, L., & Homburger, V. (2013). Shank3-Rich2 interaction regulates AMPA receptor recycling and synaptic long-term potentiation. *Journal of Neuroscience*, 33(23), 9699–9715. <https://doi.org/10.1523/JNEUROSCI.2725-12.2013>
- Sala, C., Pièch, V., Wilson, N. R., Passafaro, M., Liu, G., & Sheng, M. (2001). Regulation of dendritic spine morphology and synaptic function by Shank and Homer. *Neuron*, 31(1), 115–130. [https://doi.org/10.1016/S0896-6273\(01\)00339-7](https://doi.org/10.1016/S0896-6273(01)00339-7)
- Sarowar, T., & Grabrucker, A. M. (2016). Actin-Dependent Alterations of Dendritic Spine Morphology in Shankopathies. In *Neural Plasticity* (Vol. 2016). Hindawi Limited. <https://doi.org/10.1155/2016/8051861>
- Schindelin, J., Arganda-Carreras, I., Frise, E., Kaynig, V., Longair, M., Pietzsch, T., Preibisch, S., Rueden, C., Saalfeld, S., Schmid, B., Tinevez, J. Y., White, D. J., Hartenstein, V., Eliceiri, K., Tomancak, P., & Cardona, A. (2012). Fiji: An open-source platform for biological-image analysis. In *Nature Methods* (Vol. 9, Issue 7, pp. 676–682). Nature Publishing Group. <https://doi.org/10.1038/nmeth.2019>
- Sheng, M., & Kim, E. (2000). The Shank family of scaffold proteins. *Journal of Cell Science*, 113(11), 1851–1856. <https://doi.org/10.1242/jcs.113.11.1851>
- Song, B., Lai, B., Zheng, Z., Zhang, Y., Luo, J., Wang, C., Chen, Y., Woodgett, J. R., & Li, M. (2010). Inhibitory phosphorylation of GSK-3 by CaMKII couples depolarization to neuronal survival. *Journal of Biological Chemistry*, 285(52), 41122–41134. <https://doi.org/10.1074/jbc.M110.130351>
- Tanaka, H., & Hirano, T. (2012). Visualization of Subunit-Specific Delivery of Glutamate Receptors to Postsynaptic Membrane during Hippocampal Long-Term Potentiation. *Cell Reports*, 1(4), 291–298. <https://doi.org/10.1016/J.CELREP.2012.02.004>
- Tao-Cheng, J. H., Yang, Y., Bayer, K. U., Reese, T. S., & Dosemeci, A. (2014). NMDA-induced accumulation of Shank at the postsynaptic density is mediated by CaMKII. *Biochemical and Biophysical Research Communications*, 450(1), 808–811. <https://doi.org/10.1016/j.bbrc.2014.06.049>
- Tu, J. C., Xiao, B., Naisbitt, S., Yuan, J. P., Petralia, R. S., Brakeman, P., Doan, A., Aakalu, V. K., Lanahan, A. A., Sheng, M., & Worley, P. F. (1999). Coupling of mGluR/Homer and PSD-95 complexes by the Shank family of postsynaptic density proteins. *Neuron*, 23(3), 583–592. [https://doi.org/10.1016/S0896-6273\(00\)80810-7](https://doi.org/10.1016/S0896-6273(00)80810-7)
- Uchino, S., Wada, H., Honda, S., Nakamura, Y., Ondo, Y., Uchiyama, T., Tsutsumi, M., Suzuki, E., Hirasawa, T., & Kohsaka, S. (2006). Direct interaction of post-synaptic density-95/Dlg/ZO-1 domain-containing synaptic molecule Shank3 with GluR1 α -amino-3-hydroxy-5-methyl-4-isoxazole propionic acid receptor. *Journal of Neurochemistry*, 97(4), 1203–1214. <https://doi.org/10.1111/j.1471-4159.2006.03831.x>
- Wan, L., Liu, D., Xiao, W. B., Zhang, B. X., Yan, X. X., Luo, Z. H., & Xiao, B. (2021). Association of SHANK Family with Neuropsychiatric Disorders: An Update on Genetic and Animal Model Discoveries. In *Cellular and*

Molecular Neurobiology (pp. 1–21). Springer. <https://doi.org/10.1007/s10571-021-01054-x>

Wang, L., Pang, K., Han, K., Adamski, C. J., Wang, W., Lingjie He, •, Lai, J. K., Vitaliy, •, Bondar, V., Duman, J. G., Richman, • Ronald, Tolias, K. F., Barth, P., Palzkill, • Timothy, Liu, Z., Lloyd, • J, & Zoghbi, H. Y. (2020). An autism-linked missense mutation in SHANK3 reveals the modularity of Shank3 function. *Molecular Psychiatry*, 25, 2534–2555. <https://doi.org/10.1038/s41380-018-0324-x>

Wenthold, R. J., Petralia, R. S., Blahos, J., & Niedzielski, A. S. (1996). Evidence for multiple AMPA receptor complexes in hippocampal CA1/CA2 neurons. *Journal of Neuroscience*, 16(6), 1982–1989. <https://doi.org/10.1523/jneurosci.16-06-01982.1996>